A Diagnostic Equation for Tendency of Lapse-Rate-Tropopause Heights and Its Application

MASASHI KOHMA AND KAORU SATO

Department of Earth and Planetary Science, Graduate School of Science, The University of Tokyo, Tokyo, Japan

(Manuscript received 5 March 2019, in final form 9 August 2019)

ABSTRACT

The tropopause is the boundary between the troposphere and stratosphere and is normally defined by the temperature lapse rate. Previous studies have noted that synoptic-scale and planetary-scale disturbances bring about lapse-rate-tropopause (LRT) height fluctuations on time scales from several days to several years. In the present study, a diagnostic expression for the tendency of LRT height is derived by assuming that the LRT can be characterized as a discontinuity in the vertical gradient of the potential temperature. In addition, the contribution from each term in the thermodynamic equation to the LRT height is quantified. The derived equation is validated by examining the time variation of the LRT height associated with baroclinic waves in an idealized numerical calculation, that of the zonal-mean LRT height in GPS radio occultation data, and that of the LRT height in reanalysis data.

1. Introduction

The tropopause is the boundary between the troposphere and stratosphere. The conventional definition of the tropopause is based on the temperature lapse rate; "the lowest level at which the lapse rate decreases to $2\,\mathrm{K\,km^{-1}}$ or less, provided that the average lapse rate between this level and all higher levels within 2 km does not exceed $2\,\mathrm{K\,km^{-1}}$" (WMO 1957). The tropopause as determined under this definition is hereinafter called the lapse-rate tropopause (LRT). Across the tropopause, rapid changes in the potential vorticity (PV) and the concentrations of ozone, water vapor, and other chemical tracers are observed (e.g., Bethan et al. 1996; Hegglin et al. 2009). Previous studies (e.g., Birner et al. 2002; Birner 2006) showed that the changes across the tropopause averaged in the vertical coordinate relative to the local LRT height is sharper than those averaged in the coordinate relative to the ground level. Based on the sharp gradient for these quantities across the LRT, other definitions for the tropopause have also been suggested (e.g., PV-based tropopause, which is also known as dynamical tropopause; Hoskins et al. 1985). Nevertheless, the LRT is the most commonly used definition because it can be determined from a single vertical temperature profile. Another thermal tropopause definition is the cold-point tropopause (CPT), which is defined as the altitude where the temperature is minimized in the vertical direction. The CPT is frequently used for studies on water vapor transport associated with tropical upwelling. Pan et al. (2018) examined trace gas measurements in the tropical tropopause region and showed that the LRT is related to a sharper transition level of the species from the troposphere to the stratosphere than the CPT.

The question of what determines the tropopause height has been investigated in previous studies. Held (1982) proposed a constraint relating the tropopause height with the tropospheric stratification under the assumptions that the time-mean and zonal-mean stratification in the troposphere is constant and that the thermal structure in the stratosphere is determined by radiative equilibrium. Furthermore, in order to address this problem, he introduced additional constraints concerning dynamical entropy transport in the troposphere. Although Held's approach is highly simplified, it provides a reasonable estimate of the tropopause height (100–200 hPa in the tropics and ~400 hPa in the extratropics). This tropopause determination is based on the concept that the tropopause may be regarded as the top

Denotes content that is immediately available upon publication as open access.

Corresponding author: Masashi Kohma, kohmasa@eps.s.u-tokyo.ac.jp

DOI: 10.1175/JAS-D-19-0054.1

of the boundary layer in which the heat received at the surface is redistributed by the air motion (Schneider 2004; Zurita-Gotor and Vallis 2013). Many subsequent studies have investigated the roles of processes that were not considered by Held (1982) in determining the time-mean tropopause height. These processes include moisture effects (Thuburn and Craig 1997; Frierson et al. 2006), active roles of the stratosphere such as the meridional circulation and the shortwave heating due to ozone (Thuburn and Craig 2000), and sharp vertical gradients in longwave cooling due to water vapor (Hartmann et al. 2001; Randel et al. 2007a; Thompson et al. 2017).

While Held's approach considers the time-mean (equilibrium) state of the tropopause, there is also a temporal variability of the tropopause height associated with a variety of atmospheric processes with a wide range of time scales. For example, the (anti) cyclonic PV anomaly around the tropopause lowers (raises) LRT heights (Hoskins et al. 1985; Wirth 2000; Tomikawa et al. 2006), the activity of the storm track is connected to the zonal-mean LRT height (Son et al. 2007), and the day-to-day variation of the local tropopause level is correlated with that of the total ozone column (Steinbrecht et al. 1998). Several studies have suggested that the variability of the overturning meridional circulation in the stratosphere has an impact on the monthly mean zonal-mean LRT height (e.g., Yulaeva et al. 1994; Grise et al. 2010; Li and Thompson 2013; Kohma and Sato 2014; Barroso and Zurita-Gotor 2016). Interannual variability including the stratospheric equatorial quasi-biennial oscillation has an impact on the tropical tropopause heights (Randel et al. 2000; Grise et al. 2010).

Several previous studies have tried to quantify the time variation of tropopause heights. Son et al. (2007) examined the heat budget around the tropopause in the extratropics on intraseasonal time scales. They pointed out the importance of the lower-stratospheric temperature anomalies for the LRT height fluctuations, based on composite analyses. Barroso and Zurita-Gotor (2016) decomposed the intraseasonal variability of zonal-mean tropopause heights into low- and high-frequency components using principle component analysis and discussed the relation of the variability to wave breaking and the strength of the polar vortex.

Although the time variation of the tropopause heights on various time scales has been examined, few previous have studies considered an expression for the tropopause height explicitly. Johnson (1986) presented a simplified expression for the tropical tropopause as an infinitesimal transition layer of dry static energy s:

$$\frac{\partial z_T}{\partial t} = \overline{w} - \frac{\overline{w's'}|_{z_T-0}}{[s]^{\mathrm{St}}_{\mathrm{Tr}}} + \frac{[F_R]^{\mathrm{St}}_{\mathrm{Tr}}}{\rho[s]^{\mathrm{St}}_{\mathrm{Tr}}}, \tag{1}$$

where z_T, w, $\overline{w's'}|_{z_T-0}$, F_R, and ρ are the tropopause height, vertical velocity, heat flux at the bottom of the transition layer, radiative heating rate, and density, respectively. The square brackets $[\cdot]^{\mathrm{St}}_{\mathrm{Tr}}$ indicate a jump across the transition layer. The overbar refers to the area average. Johnson (1986) derived Eq. (1) from an analogy with an equation for the depth of the convective boundary layer, which is derived under the assumption that there is a jump in the virtual potential temperature at the top of the boundary layer (e.g., Lilly 1968; Zeman and Tennekes 1977). The validity of Eq. (1) is not discussed in detail for the real atmosphere in Johnson (1986), however.

In the present study, we simplify the tropopause to a discontinuity in the vertical gradient of the potential temperature, which is a traditionally used assumption in previous studies on tropopause dynamics (e.g., Juckes 1994, 1997), and derive a diagnostic relation for the tendency in the tropopause height. This type of procedure is used for analyses of nonlinear waves, for example, when calculating the propagation speed of shock waves (Tanaka 2017). We applied the derived relation to model simulation, observational data, and reanalysis data in order to evaluate the accuracy of the derived equation. It is known that the tropopause height is affected by various physical processes (e.g., Randel and Jensen 2013). The equation proposed in the present study has a potential to quantify which physical processes are important for the seasonal and long-term changes in the tropopause heights. For example, it is possible to quantitatively answer questions such as whether the cause of the decrease in the polar tropopause height during sudden stratospheric warming (e.g., Kohma and Sato 2014) can be explained by the enhancement of the downward residual mean flow in the polar region, or what causes the intermodel variability in the trend and interannual variability of the tropopause height (Gettelman et al. 2010; Hegglin et al. 2010).

Note that recent observational studies have revealed that a thin but finite-depth unique vertical structure is observed around the tropopause in both the tropics and extratropics, which are known as the tropical tropopause layer (TTL) and extratropical transition layer (ExTL), respectively (Fueglistaler et al. 2009b; Gettelman et al. 2011). Birner et al. (2002) considered the climatological features in the inversion layer just above the tropopause (TIL) in the extratropics. The findings of these studies suggest that the tropopause is characterized as a finite-depth layer rather than as a boundary at a specific height. In this context, the present tropopause model may be an oversimplification. It is shown later that, nevertheless, the derived equation explains much of the

variance in the LRT heights tendency in the observational and model data under certain conditions.

This study is organized as follows. The derivation of diagnostic expression for the tendency of tropopause height is given in section 2. The applications of the derived equation to simple baroclinic instability in a numerical experiment, GPS radio occultation (GPS RO) observation data, and reanalysis data are presented in sections 3, 4, and 5, respectively. The summary and concluding remarks are given in section 6.

2. Derivation of tendency equation for LRT heights

To derive the tendency equation for the LRT height $z_T(x, y, t)$, a simplified representation of the tropopause as a discontinuity in the vertical gradient of potential temperature is used. Specifically, we make two assumptions for the tropopause: (i) potential temperature $\theta(x, y, z, t)$ is continuous in the vertical direction and smooth except at an altitude of z_T and (ii) $\theta_z(x, y, z, t)$ is continuous and smooth except at altitude z_T and has a discontinuity at z_T, where the suffix z denotes the partial derivative in z. The validity of the posed assumptions will be discussed in section 2a. Figure 1 shows a schematic of the simplified vertical structures of θ and θ_z around the tropopause. This kind of simplification is known as shock fitting. Thus, the following relations hold around z_T:

$$\theta[x,y,z_T(x,y,t)+0,t]-\theta[x,y,z_T(x,y,t)-0,t]=0, \quad (2)$$

$$\theta_z[x,y,z_T(x,y,t)+0,t]-\theta_z[x,y,z_T(x,y,t)-0,t] = S(>0), \quad (3)$$

where $f(z_T+0)\equiv\lim_{z\searrow z_T} f(z)$ and $f(z_T-0)\equiv\lim_{z\nearrow z_T} f(z)$. Note that S is known as the sharpness of the tropopause (e.g., Bethan et al. 1996; Zängl and Hoinka 2001). The Euler derivative of Eq. (2) gives

$$\begin{aligned}&\theta_t[x,y,z_T(x,y,t)+0,t]+\frac{\partial z_T}{\partial t}\theta_z[x,y,z_T(x,y,t)+0,t]\\&\quad-\theta_t[x,y,z_T(x,y,t)-0,t]\\&\quad-\frac{\partial z_T}{\partial t}\theta_z[x,y,z_T(x,y,t)-0,t]=0,\\&\therefore-[\theta_t]^{\mathrm{St}}_{\mathrm{Tr}}=\frac{\partial z_T}{\partial t}S,\end{aligned}$$

where $[f]^{\mathrm{St}}_{\mathrm{Tr}}\equiv f(x, y, z_T+0, t)-f(x, y, z_T-0, t)$ for an arbitrary function $f(x, y, z, t)$ indicates a jump across the tropopause. The suffix t denotes the Euler derivative. Note that S is rewritten as $[\theta_z]^{\mathrm{St}}_{\mathrm{Tr}}$. Thus, using $S>0$, the diagnostic relation for the tendency of z_T can be written as

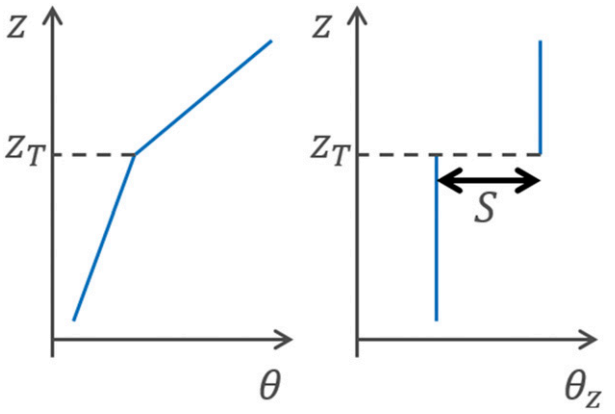

FIG. 1. A schematic illustration of the vertical profiles of θ and θ_z around the tropopause height z_T, which are considered in the present study. The jump in θ_z across z_T is expressed as S.

$$\frac{\partial z_T}{\partial t}=-\frac{[\theta_t]^{\mathrm{St}}_{\mathrm{Tr}}}{S}. \quad (4)$$

The right-hand side of Eq. (4) is expressed as the difference between the Euler derivative of the potential temperature across the tropopause $[\theta_t]^{\mathrm{St}}_{\mathrm{Tr}}$ and sharpness S. This relation corresponds to the Hugoniot–Duhem theorem for a first-order discontinuity. Another but equivalent derivation of Eq. (4) using Leibniz's integral rule is also provided in the appendix.

It should be noted that the WMO's definition of the LRT is based on a specific value of the lapse rate ($2\,\mathrm{K\,km^{-1}}$) although the tropopause in the present study is defined as a discontinuity of the lapse rate. Thus, strictly speaking, the tendency of LRT heights in the present study is not the same as those based on the WMO's definition. Nevertheless, observational studies (e.g., Birner et al. 2002) have also considered the climatological features for a sharp change of the vertical gradient of θ across the LRT except in the polar winter region. This point is discussed in more detail in section 2a.

The right-hand side of Eq. (4) is rewritten using the thermodynamics equation ($\theta_t = Q - \mathbf{v}\cdot\nabla\theta$, where Q is the diabatic heating rate for θ, and the thermal diffusion is neglected):

$$\frac{\partial z_T}{\partial t}=-\frac{[Q-(\mathbf{v}\cdot\nabla\theta)]^{\mathrm{St}}_{\mathrm{Tr}}}{S}. \quad (5)$$

Here, Eq. (5) is a more general form of Eq. (1), based on a discontinuity in θ_z. It should also be emphasized that the tendency of z_T due to adiabatic/diabatic processes can be evaluated separately using Eq. (5). Specifically, the first term associated with Q on the right-hand side of Eq. (5) corresponds to the contribution from diabatic processes while the second term expresses

that from adiabatic (i.e., advective) processes. Because both terms are divided by S, large values of S lead to a decrease in the absolute value of the change in the LRT height. Note that the LRT heights have to be provided to calculate the tendency using Eq. (4) and/or Eq. (5) since the operation $[\cdot]_{\mathrm{Tr}}^{\mathrm{St}}$ includes the LRT heights.

It should be noted that Eq. (4) is a kinematic relation; namely, there is no need to specify the governing equations including spatial coordinates in the derivation of Eq. (4). Thus, the tendency equation for temporal-mean and/or spatial-mean z_T can be obtained in the same manner as long as the two assumptions [Eqs. (2) and (3)] are satisfied. For example, using the transformed-Eulerian-mean equation system (TEM system; Andrews et al. 1987), the tendency equation for the LRT height in the TEM system is derived as follows:

$$\frac{\partial \overline{z}_T}{\partial t} = -\frac{[\overline{\theta}_t]_{\mathrm{Tr}}^{\mathrm{St}}}{\overline{S}}, \tag{6}$$

where the overbar indicates the zonal mean. Note that the zonal mean will smooth sharp changes of θ_z (Birner 2006), and thus the assumption of discontinuities in θ_z should be validated carefully.

Furthermore, by combining with the thermodynamic equation in the TEM system, Eq. (6) can be rewritten as follows if the diffusion effect is neglected:

$$\frac{\partial \overline{z}_T}{\partial t} = -\frac{[\overline{Q} - (\overline{\mathbf{v}}^* \cdot \nabla)\overline{\theta} - (1/\rho_0)(\partial G/\partial z)]_{\mathrm{Tr}}^{\mathrm{St}}}{\overline{S}}, \tag{7}$$

where $\overline{\mathbf{v}}^* \equiv (0, \overline{v}^*, \overline{w}^*)$ is the residual mean velocity vector and $G \equiv \rho_0(\overline{v'\theta'}\overline{\theta}_y + \overline{w'\theta'}\overline{\theta}_z)/\overline{\theta}_z$, which becomes zero for linear, adiabatic, steady disturbances or the quasigeostrophic limit. The primes denote the perturbations from the zonal mean. This equation corresponds to the TEM version of Eq. (5).

Before proceeding to the application of the derived equations to atmospheric data, we discuss briefly the assumptions used in the derivation and their applicability.

a. On assumptions in use

For deriving the master relation of the tendency of LRT heights [Eq. (4)], we make the following two assumptions [Eqs. (2) and (3)]: θ is continuous, and there is a discontinuity in θ_z at the tropopause level. The former seems to be a valid assumption for the real atmosphere [Fig. 3 in Gettelman et al. (2011)]. For the assumption on θ_z, rapid changes across the tropopause are commonly observed (Schmidt et al. 2005; Grise et al. 2010; Son et al. 2011) except in the polar winter region. Previous studies have investigated the sharpness of the tropopause in terms of the contrast of θ_z between above and below tropopause. In the polar winter, the contrast across the tropopause is weak (Zängl and Hoinka 2001). When the sharpness approaches zero, the right-hand side of Eq. (4) becomes infinite. The LRT is frequently undetectable in the Antarctic winter for the same reason (e.g., Pan and Munchak 2011). Thus, the application of Eq. (4) or Eq. (5) is not meaningful for the polar winter region.

In the derivation of the relation for the tendency of the LRT height, it is implicitly assumed that the vertical profile has a single discontinuity in θ_z. Accordingly, the presence of multiple discontinuities, corresponding to multiple tropopause structures, is neglected in the present configuration. As a result, it may be problematic to apply the derived equation when multiple tropopauses are present, for example, during tropopause folding events at the midlatitudes (e.g., Keyser and Shapiro 1986; Danielsen et al. 1991), tropopause breaks around the subtropical jet (Randel et al. 2007b), and strong temperature fluctuations associated with intense inertia–gravity waves in the polar winter (Shibuya et al. 2015). The applicability of the derived relation to multiple tropopauses will be shown briefly in section 5.

b. Applicability to observational and model data

To assess the accuracy of the right-hand side of Eqs. (4)–(7), datasets with a very high vertical resolution are desirable since the operation $[\cdot]_{\mathrm{Tr}}^{\mathrm{St}}$ is defined as the difference across the infinitesimal transition layer. It is not always possible to make use of high-vertical-resolution data. For practical applications, we have to approximate the operation as a finite difference across the tropopause:

$$[f]_{\mathrm{Tr}}^{\mathrm{St}} \approx [f]_{z_0}^{z_1} \equiv f(z_1) - f(z_0), \tag{8}$$

where $z_0 < z_T < z_1$.

Note that variations in θ or θ_z with vertical wavelengths shorter than a distance between z_0 and z_1 may cast doubt on the validity of the approximation. The validity of the approximation should be confirmed by comparing the left-hand side of Eq. (4) to an approximation of the right-hand side (i.e., $\partial z_T/\partial t \approx -[\theta_t]_{z_0}^{z_1}/S$). If the equality holds, then this is an indicator of not only the validity of the finite-difference approximation, but also that of the simplification of the tropopause as a discontinuity in θ_z.

3. Application to baroclinic instability in a simplified model

First, we applied the derived relation to the results of a numerical experiment for baroclinic instability in dry, adiabatic atmosphere introduced by Polvani et al. (2004).

a. Numerical model and experiment setup

The Dennou-Club Planetary Atmospheric Model, version 5 (DCPAM5; Takahashi et al. 2018), is used for numerical calculation of baroclinic instability in a dry, adiabatic atmosphere in spherical coordinates. DCPAM5 is an atmospheric general circulation model, whose dynamical core is a hydrostatic spherical spectral model. In the experiment, a horizontally triangularly truncated spectral resolution of T85 is used. The vertical coordinate is comprised of 40 σ levels.

The experiment setup follows Polvani et al. (2004). The basic flow is given as a zonally symmetric zonal flow. Figure 2 shows latitude–pressure sections of the basic zonal flow and potential temperature, which is balanced with the zonal flow through the thermal wind relation. The black broken curve indicates z_T for the basic state. The values of z_T are obtained by applying the method of Reichler et al. (2003), which is developed for deriving the tropopause height from relatively coarse-resolution temperature data using interpolation of lapse rates. The obtained LRT height is hereinafter referred to as the observed z_T. Although z_T in the tropics (~200 hPa) is quite low compared to the real atmosphere, it is observed that the tropical z_T is higher than that in the extratropics. To induce the development of baroclinic eddies, a small temperature perturbation is added around 45°N. Polvani et al. (2004) showed that eddies similar to LC1 (Thorncroft et al. 1993) develop in this experiment setup. Diffusion terms are included in the momentum and thermodynamic equations to avoid developing sharp fronts in a short time period (Polvani et al. 2004). The numerical integration is performed over 12 days and the results for day 12 are shown below. The temporal tendency of tropopause height is calculated from the forward difference in z_T at 0000 UTC on day 12 divided by 1 h.

b. Results

Figure 3a shows a horizontal map of z_T (color) on day 12 together with the relative vorticity at 250 hPa (contours). It is observed that negative and positive z_T anomalies from the background correspond to cyclonic and anticyclonic relative vorticity anomalies, respectively. The balanced relation between tropopause heights and potential vorticity anomalies around the tropopause has already been discussed in many previous studies (e.g., Hoskins et al. 1985; Wirth 2000). Note that the signature of double tropopause is not found within the present integration time period. Figure 3b shows the tendency of the LRT height ($\partial z_T/\partial t$). The peak-to-peak amplitude is about 1.1 km day^{-1} at most.

To apply the tendency equation for LRT heights, it is necessary to specify the two levels which sandwich the tropopause [z_0 and z_1 in Eq. (8)]. Because the tropopause heights range from 9.5 to 11 km (260–210 hPa in pressure) in Fig. 3b, the upper (lower) level should be higher (lower) than 210 (260) hPa. Here we chose the upper level as 190 hPa, which corresponds to the lowest model level higher than 210 hPa. Similarly, the lower level is chosen as 290 hPa. Figure 3c shows a horizontal map of the tendency of LRT heights estimated from the RHS of Eq. (4) (viz., $-[\theta_t]_{z_0}^{z_1}/S$) on day 12. The plot indicates that the horizontal distribution of the LRT height tendency estimate is in good agreement with that of the observed tendency. The difference at 45°N is 0.1 km day^{-1} at most.

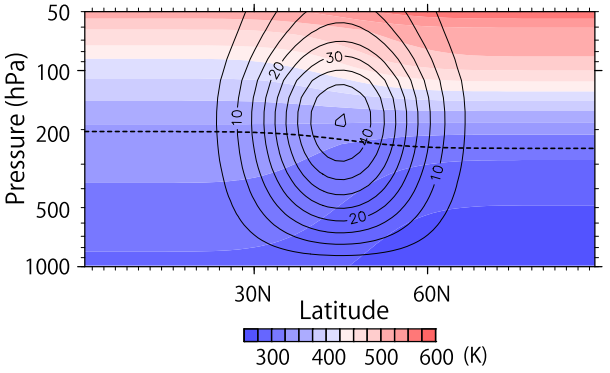

FIG. 2. The initial zonal wind (contours; interval: 5 m s^{-1}) and potential temperature (colors). The dashed line indicates LRT heights.

From Eq. (5), the contribution of each term in the thermodynamic equation can be evaluated. The contributions of the vertical and horizontal advection terms are shown in Figs. 4a and 4b, respectively. Note that because θ_t is equal to $(\mathbf{v} \cdot \nabla)\theta$ except for the numerical diffusion term in the present experiment, the summation of Figs. 4a and 4b is almost identical to Fig. 3c. The contribution from the vertical advection has opposite sign to that from the horizontal advection while the amplitude of the contribution from the horizontal advection is approximately twice as large as that of the vertical advection. It is reasonable to expect the compensation between the horizontal and vertical advection because, when the flow is quasigeostrophic, the (ageostrophic) vertical motion is determined by keeping the flow in approximate thermal wind balance (Holton and Hakim 2012). Figure 4c shows the contribution of the ageostrophic flow. The westward shift of the positive (negative) tendency associated with the ageostrophic flow is observed against the positive (negative) anomalies in the tropopause level (Fig. 3a), which can be understood in terms of the intrinsic phase speed of Rossby waves.

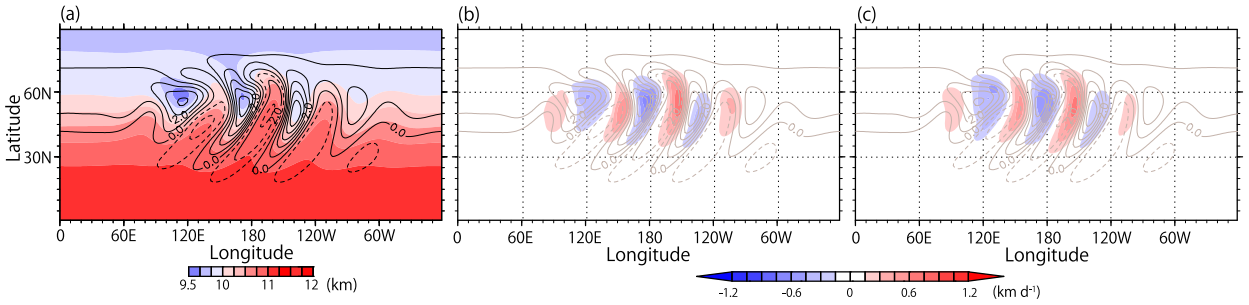

FIG. 3. Results for the numerical calculation of the idealized baroclinic instability on day 12. (a) Relative vorticity at 250 hPa (contours; negative dashed; interval: $1.0 \times 10^{-5}\,\mathrm{s}^{-1}$) and LRT height (color). (b) Tendency of LRT height ($\partial z_T/\partial t$; colors) and relative vorticity at 250 hPa (contours). (c) As in (b), but for estimates from Eq. (4) ($-[\theta_t]_{z_0}^{z_1}/S$; colors).

We also performed numerical experiments with different horizontal resolutions (T21, T42, and T170) and vertical resolutions (L20 and L60) and confirmed that the above results are not much changed (not shown here). In summary, from the numerical experiments for idealized baroclinic instability, it is confirmed that the tendency of LRT heights estimated from the derived equation accords well with the observed value. This means that Eq. (5) [and hence Eq. (4)] provides a quantitative evaluation of the contribution from each term in the thermodynamic equation to the change in the LRT height.

4. Application to GPS RO observations

Next, results for the application of our equations to the GPS RO observational data are shown. We focus on zonal-mean LRT heights in finite latitudinal ranges because the locations of GPS RO observations vary with time. Through a comparison of the tendency of the zonal-mean LRT heights $\partial z_T/\partial t$ with $-[\theta_t]_{z_0}^{z_1}/S$, it is possible to test the validity of (i) the simplified representation where the tropopause is regarded as the level of the discontinuity of θ_z and (ii) the approximation of the limit operation with the finite difference ($[\cdot]_{\mathrm{Tr}}^{\mathrm{St}} \approx [\cdot]_{z_0}^{z_1}$).

a. Data and analyses

The GPS RO data from the Constellation Observing System for Meteorology, Ionosphere and Climate/*Formosa Satellite 3* (COSMIC/*FORMOSAT3*) are used. The dry temperature with a vertical resolution of about 100 m from the GPS RO observation is analyzed (Anthes et al. 2008). The dry temperature profiles are calculated from the observed refractivity under the assumption that the contributions of water vapor pressure and electron density are negligible. The accuracy of the dry temperature data is better than 0.5 K in the altitude range of 10–20 km and is about 0.5 K above an altitude range of 6–8 km (Schreiner et al. 2007; Shepherd and Tsuda 2008). The data are interpolated to intervals of 200 m to make the analysis easier. We adopted the algorithm for determining the first LRT height from the GPS RO measurements which was proposed by Schmidt et al. (2005). In the present study, 7 years of observational data (2007–13) are analyzed, which includes about 1600 vertical profiles per day on average.

Zonal-mean z_T ($\overline{z}_T$) are calculated daily for each hemisphere in eight latitudinal ranges: 0°–10°, 10°–20°, 20°–30°, 30°–40°, 40°–50°, 50°–60°, 60°–70°, and 70°–90°. The period analyzed for the latitude range of 90°–50°S is limited to November–May since the LRT is often

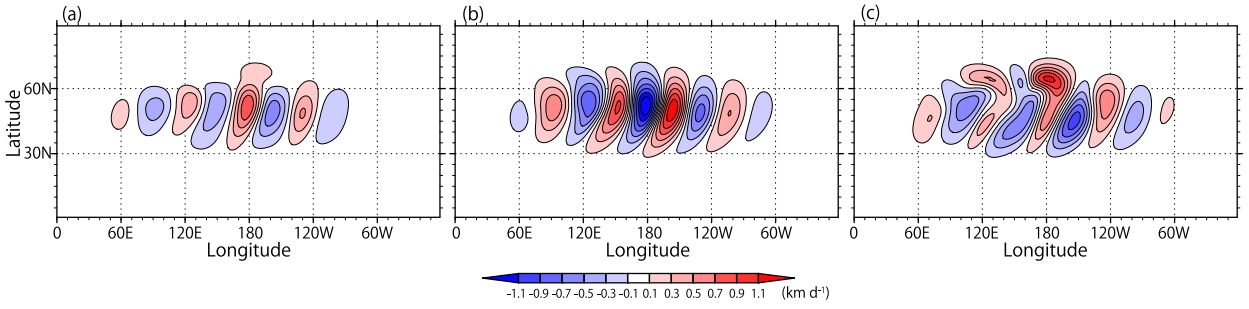

FIG. 4. As in Fig. 3c, but for contributions from (a) vertical advection ($-[w\theta_z]_{z_0}^{z_1}/S$), (b) horizontal advection ($-[\mathbf{u}\cdot\nabla_H\theta]_{z_0}^{z_1}/S$), and (c) ageostrophic flow $\{-[(\mathbf{v}_a\cdot\nabla)\theta]_{z_0}^{z_1}/S\}$, where $\mathbf{u}$ is the horizontal wind vector, $\mathbf{v}_a = (u_a, v_a, w)$ is the ageostrophic wind, and ∇_H is the horizontal gradient operator.

undetectable there during the austral winter. Then, the obtained time series are smoothed with a low-pass filter with a cutoff length of 15 days to reduce nonuniformities in the number of observations. Small structures in vertical profiles of θ, which are associated with a variety of physical processes including frontal structures, gravity waves, and convection are considerably smoothed by the spatial and temporal filters.

b. Results

Figure 5 shows raw and smoothed time series of $\overline{z}_T$ for 2009 in 0°–10°, 40°–50°, and 70°–90°N. We focus on the smoothed time series in the following analyses. In the tropics, high $\overline{z}_T$ (~17 km) is observed in November–March and then descends to about 16 km in June. The seasonal variation of LRT height in the tropics is considered to be a reflection of the strength of upwelling in the TTL driven by extratropical and equatorial waves (Yulaeva et al. 1994; Norton 2006; Randel et al. 2008). Subseasonal variability in $\overline{z}_T$ is also observed, in particular, in January–February and July–October. In the midlatitude region, $\overline{z}_T$ shows a clear seasonal cycle having a peak (~14 km) in the boreal summer and a minimum (~10 km) in the boreal winter. This feature likely corresponds to the seasonality of the Hadley cell, whose poleward branch extends northward in the boreal summer. The Arctic $\overline{z}_T$ has a seasonal variation similar to that in the midlatitude region while a rapid descent is observed in late January. The rapid descent in late January is associated with sudden stratospheric warming (e.g., Kohma and Sato 2014).

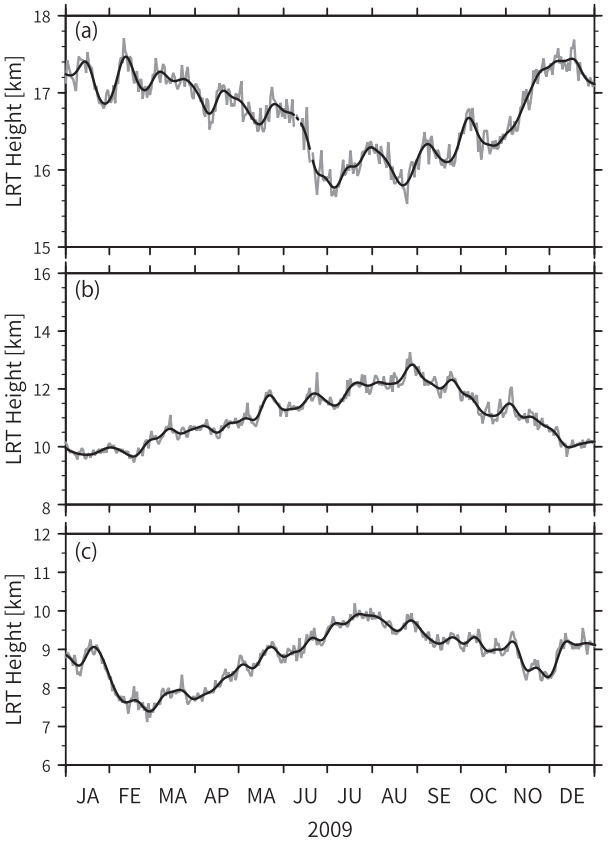

FIG. 5. Time series of raw (gray curves) and smoothed (black curves) $\overline{z}_T$ in 2009 in the latitude ranges of (a) 0°–10°, (b) 40°–50°, and (c) 70°–90°N.

As mentioned in sections 2b and 3b, in order to evaluate the RHS of Eq. (6), the two levels that sandwich the LRT have to be specified. In the following, a diagnosis using fixed altitudes, which is the same as in section 3, and that using a fixed distance from $\overline{z}_T(y, t)$ are shown. The latter is written as $-[\overline{\theta}_t]^{\overline{z}_T+\Delta z_1}_{\overline{z}_T+\Delta z_0}/\overline{S}$, where Δz_0 and Δz_1 are distances from the zonal-mean LRT heights and the denominator $\overline{S}$ is evaluated as $[\overline{\theta}_z]^{\overline{z}_T+\Delta z_1}_{\overline{z}_T+\Delta z_0}$. The levels z_0 and z_1 were chosen such that the mean square of the difference between $\partial\overline{z}_T/\partial t$ and $-[\overline{\theta}_t]^{z_1}_{z_0}/\overline{S}$ was minimized for each latitudinal range. Similarly, the relative distance Δz_0 and Δz_1 were determined so that the mean square of the difference between $\partial\overline{z}_T/\partial t$ and $-[\overline{\theta}_t]^{\overline{z}_T+\Delta z_1}_{\overline{z}_T+\Delta z_0}/\overline{S}$ was minimized.

The levels used for the diagnostics are shown in Fig. 6. Both z_0 and z_1 have maxima in the tropics and lower values in the extratropics. It is likely that z_0 and z_1 correspond to the envelope of the spatial/temporal variation of the LRT heights as a function of latitude. The distance between z_0 and z_1 in 20°–30° for both hemispheres is maximized. The largest distance for the chosen levels for the coordinate relative to zonal-mean LRT is also observed in 20°–30°. Note that it was confirmed that the following results do not change significantly if z_0, z_1, Δz_0, and/or Δz_1 are displaced by 0.2 km.

Figure 7 shows time series of $\partial\overline{z}_T/\partial t$, $-[\overline{\theta}_t]^{z_1}_{z_0}/\overline{S}$, and $-[\overline{\theta}_t]^{\overline{z}_T+\Delta z_1}_{\overline{z}_T+\Delta z_0}/\overline{S}$ in 2009 in 0°–10°, 40°–50°, and 70°–90°N. It is found that both estimates are in good agreement with $\partial\overline{z}_T/\partial t$ in all three latitude ranges in many aspects: for example, subseasonal variation in January–February and July–October in the tropics, prolonged negative values (up to $-80\,\mathrm{m\,day^{-1}}$) in November–December in the midlatitude region, and large negative values ($\sim -100\,\mathrm{m\,day^{-1}}$) in the Arctic in late January. The coefficients of determination (R-squared, or contribution rate) between $\partial\overline{z}_T/\partial t$ and $-[\overline{\theta}_t]^{z_1}_{z_0}/\overline{S}$ are 0.86, 0.79, and 0.84 in 0°–10°, 40°–50°, and 70°–90°N, respectively. The R-squared values for $-[\overline{\theta}_t]^{\overline{z}_T+\Delta z_1}_{\overline{z}_T+\Delta z_0}/\overline{S}$ are 0.87, 0.84, and 0.92 in the same latitude ranges.

To describe how the real and estimated tendencies accord, the R-squared values and regression coefficients in 2007–13 are shown in Fig. 8. The R-squared values are greater than 0.64 except in the latitude range of 20°–30° in both hemispheres. The highest R-squared values are

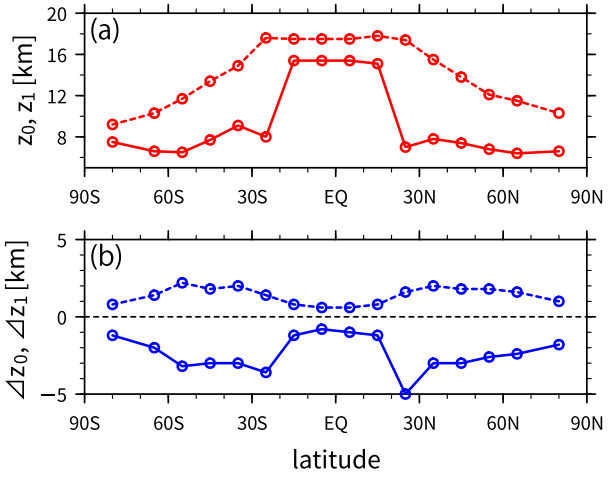

FIG. 6. (a) z_0 (red solid curve) and z_1 (red broken curve) as a function of latitude. (b) As in (a), but for Δz_0 (blue solid curve) and Δz_1 (blue broken curve). A horizontal broken line indicates a value of zero.

observed in 50°–60° (~0.94). The R-squared values for estimation from $-[\overline{\theta}_t]_{\overline{z}_T+\Delta z_0}^{\overline{z}_T+\Delta z_1}/\overline{S}$ are generally higher than those for the estimates based on fixed levels, particularly in the tropics. The R-squared values in the subtropical regions tend to be small compared to those in the other latitude ranges. To examine the validity of the assumptions used for the estimation method, examples of vertical profiles of monthly averaged $\overline{\theta}$ and $\overline{\theta}_z$ are shown as a function of height relative to $\overline{z}_T$ in Figs. 9a and 9b, respectively. The profiles are averaged over June 2009 in the latitude ranges of 0°–10°, 20°–30°, and 50°–60°N. Note that, compared to those shown in Birner et al. (2002), the profiles of $\overline{\theta}$ and $\overline{\theta}_z$ are smooth around the LRT since the time average is performed relative to the zonal-mean LRT [i.e., $\overline{z}_T(y, t)$] rather than local LRT. The obvious jump in $\overline{\theta}_z$ across the $\overline{z}_T$ is seen in 0°–10° and 50°–60°N while $\overline{\theta}_z$ in 20°–30°N changes gradually across the LRT. This indicates that the assumption on a jump in $\overline{\theta}_z$ at the LRT [i.e., Eq. (3)] is not well satisfied for 20°–30°N compared with other latitudinal ranges. Similar results are also obtained in the southern latitudes.

Regarding the regression coefficients (Fig. 8b), the both estimates in 30°S–30°N show values close to one (0.95–1.05) while the coefficients in the high latitudes (70°–90°) are relatively small (0.79–0.93). This may be related to the time variation of the static stability in the altitude range between z_0 and z_1. Previous observational studies (e.g., Randel et al. 2007a; Tomikawa et al. 2009) demonstrated large seasonal variation in the static stability around the tropopause in the polar region. Figure 9c shows monthly mean $\overline{\theta}_z$ as a function of height relative to $\overline{z}_T$ in 70°–90°N in June and December 2009. In both profiles, distinct

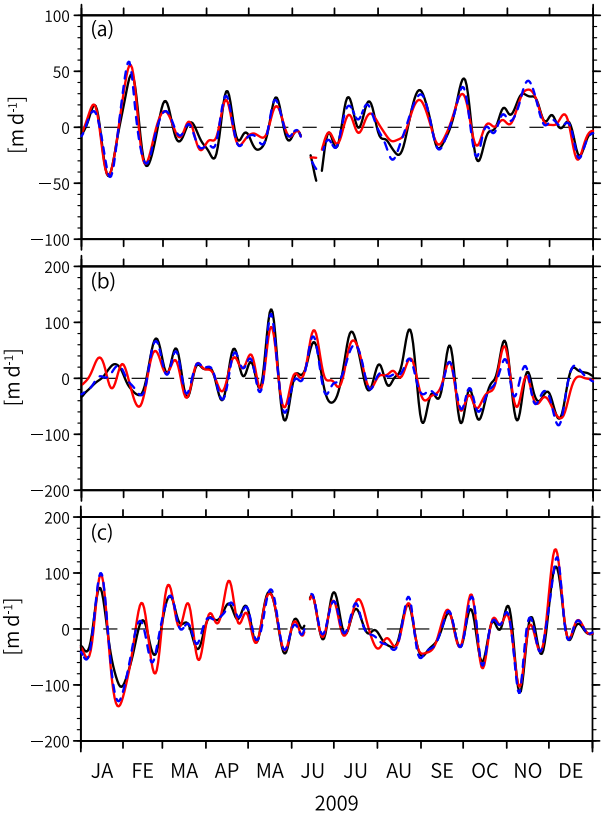

FIG. 7. As in Fig. 5, but for time series of $\partial\overline{z}_T/\partial t$ (black solid curves), $-[\overline{\theta}_t]_{z_0}^{z_1}/\overline{S}$ (red solid curves), and $-[\overline{\theta}_t]_{\overline{z}_T+\Delta z_0}^{\overline{z}_T+\Delta z_1}/\overline{S}$ (blue broken curves) in 2009. The dashed horizontal lines indicate a value of zero.

jumps in $\overline{\theta}_z$ are observed across the LRT while the maxima in $\overline{\theta}_z$ are observed about 1.6 km above $\overline{z}_T$, which corresponds to TIL, only in June. Thus, the small regression coefficients in the polar region should be attributable to the seasonal variation of $\overline{\theta}_z$ above the tropopause. In the latitude range of 30°–40°, the regression coefficients are significantly larger than 1. This is likely due to the gradual variation in $\overline{\theta}_z$ across the LRT in winter (Fig. 9d).

In the tropical regions, the CPT is well defined, and its seasonal variation is largely correlated with that of the LRT while the CPT is up to ~1 km higher than the LRT (e.g., Seidel et al. 2001). The estimates based on the coordinate relative to zonal-mean CPT in 0°–10°N are shown with the observed CPT tendency in Fig. 10. The Δz_0 and Δz_1 are chosen as −1.0 and 0.6 km, respectively, which are the same as the values for the same latitude range shown in Fig. 6. The estimated tendency accords with the CPT tendency although the R-squared value (0.74) is smaller than that for the LRT-based tendency.

Although the estimates are not perfectly accurate, the R-squared value between $\partial\overline{z}_T/\partial t$ and

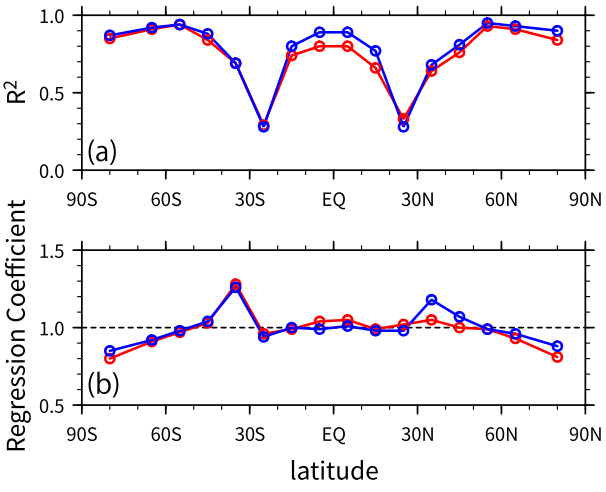

FIG. 8. (a) Coefficient of determination between the time series of $\partial\overline{z}_T/\partial t$ and $-[\overline{\theta}_t]_{z_0}^{z_1}/\overline{S}$ (red curves) and between the time series of $\partial\overline{z}_T/\partial t$ and $-[\overline{\theta}_t]_{\overline{z}_T+\Delta z_0}^{\overline{z}_T+\Delta z_1}/\overline{S}$ (blue curves). (b) As in (a), but for the regression coefficients of the regression of $\partial\overline{z}_T/\partial t$ on the estimates. The unit of the regression coefficient is (m day^{-1}) (m day^{-1})$^{-1}$.

$-[\overline{\theta}_t]_{z_0}^{z_1}/\overline{S}$ ($-[\overline{\theta}_t]_{\overline{z}_T+\Delta z_0}^{\overline{z}_T+\Delta z_1}/\overline{S}$) is higher than 0.64 (0.68) except in the latitude of 20°–30°. This means that, other than the subtropical region, the finite-difference approximation [i.e., Eq. (8)] is reasonable for estimating $-[\overline{\theta}_t]_{\mathrm{Tr}}^{\mathrm{St}}/\overline{S}$. In summary, it is found that the observed and estimated tendencies in zonal-mean LRT heights accord well far as the assumptions (2) and (3) hold.

5. Application to reanalysis data

In this section, examples of the horizontal distribution of the tropopause heights as an application to reanalysis data are shown. Here, only the results for specific four days (1 January, 1 April, 1 July, and 1 October 2009) are shown, and the results of more statistical analysis will be discussed in the future.

a. Data and analyses

The Japanese 55-year Reanalysis dataset (JRA-55; Kobayashi et al. 2015) is used for the present analyses. The data product used here is on pressure levels and 1.25° × 1.25° longitude–latitude grid, and the temporal interval is 6 h. Similar to section 3, the z_T values are obtained by applying the method of Reichler et al. (2003) to vertical temperature profiles.

To evaluate the RHS of Eq. (6), a diagnosis is performed using a fixed distance Δz from the local tropopause height $z_T(x, y, t)$. In the following analyses, the constant value of 500 m is used as Δz although the optimal value should be a function of space and time. The values of $\theta_t(z_T \pm \Delta z)$ and $\theta_z(z_T \pm \Delta z)$ are calculated from a vertical interpolation in the log-pressure coordinates for each horizontal grid point. Note that the results for $\Delta z = 1000$ m are qualitatively the same as those for $\Delta z = 500$ m.

b. Results

The left column of Fig. 11 shows horizontal maps of the observed tendency of z_T together with z_T itself. The tropopause break is observed in the subtropics of the both hemispheres. For all four days, the absolute value of the tendency tends to be larger in the extratropics than in the tropics. In addition, synoptic-scale structures predominate in the extratropics, whereas smaller-scale structures are dominant in the tropics.

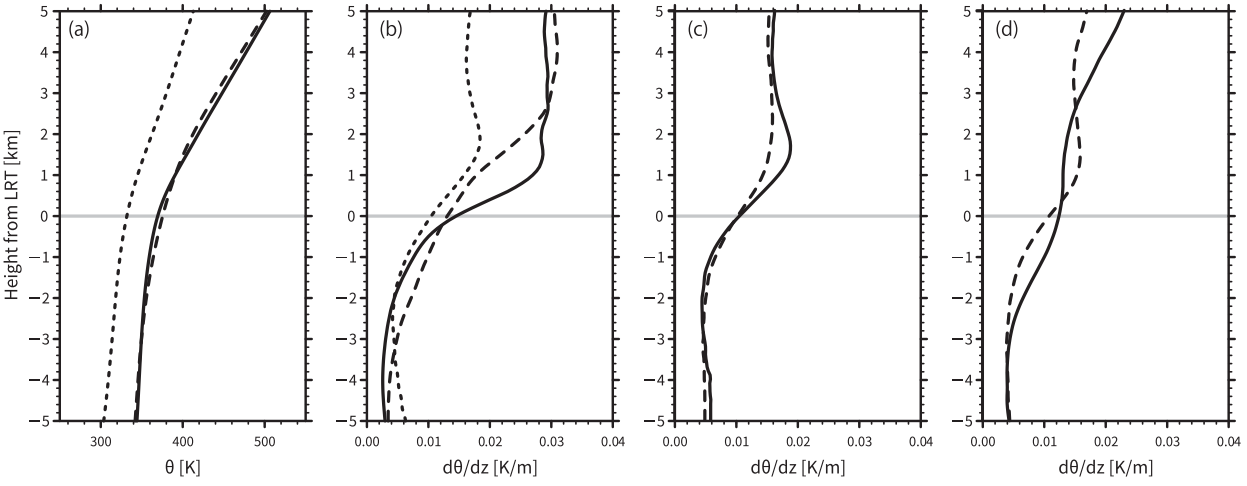

FIG. 9. (a) Vertical profiles of $\overline{\theta}$ averaged over 0°–10° (solid), 20°–30° (broken), and 50°–60°N (dotted) in June 2009. The profiles are time averaged relative to the respective $\overline{z}_T$ (horizontal gray line). (b) As in (a), but for $\overline{\theta}_z$. (c) As in (b), but for 70°–90°N in June (solid) and December (broken) 2009. (d) As in (b), but for 40°–30°S in June (solid) and December (broken) 2009.

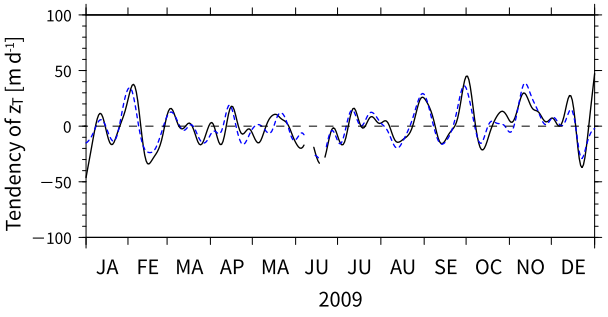

FIG. 10. As in Fig. 8a, but for time series of the observed tendency of CPT heights (black solid curves) and estimates from the derived equation (blue broken curves) in 2009.

The estimated tendency and the observed values minus estimates are shown in the center and right columns of Fig. 11, respectively. The overall distribution of the estimates qualitatively agrees well with that of the observed values. The median (mean) absolute value of the difference, calculated for every 10° latitude band, is 0.1–0.2 (0.4–0.5) km day^{-1}, except in the high latitudes of the Southern Hemisphere on 1 October and in the latitude range of 20°–40°.

Around the tropopause break, large differences between the observed and estimated tendencies are often observed. Figure 12a shows a latitude–pressure section of temperature and θ_z together with z_T in 30°–50°N, 175°W on 1 January 2009. The LRT is located around 230 hPa on the north side of 35°N while it rises up to 120 hPa on the south side. In 35°–37.5°N, small θ_z are observed above tropopause (125–150 hPa). These features suggest that the tropopause break occurs around 35°N and that the derived equation is unlikely to provide appropriate estimates there.

Even other than subtropics, significant differences between the observed and estimated tendencies are occasionally found in some regions, for example, in 45°–65°S, 45°–75°E on 1 April (Fig. 11f); in 55°–65°S, 120°E, on 1 July (Fig. 11i); and in all the longitude ranges at 60°–70°S on 1 October (Fig. 11l). Figure 12b shows a latitude–pressure section in 65°–45°S, 60°E on 1 April. There is a strong horizontal temperature gradient in the troposphere

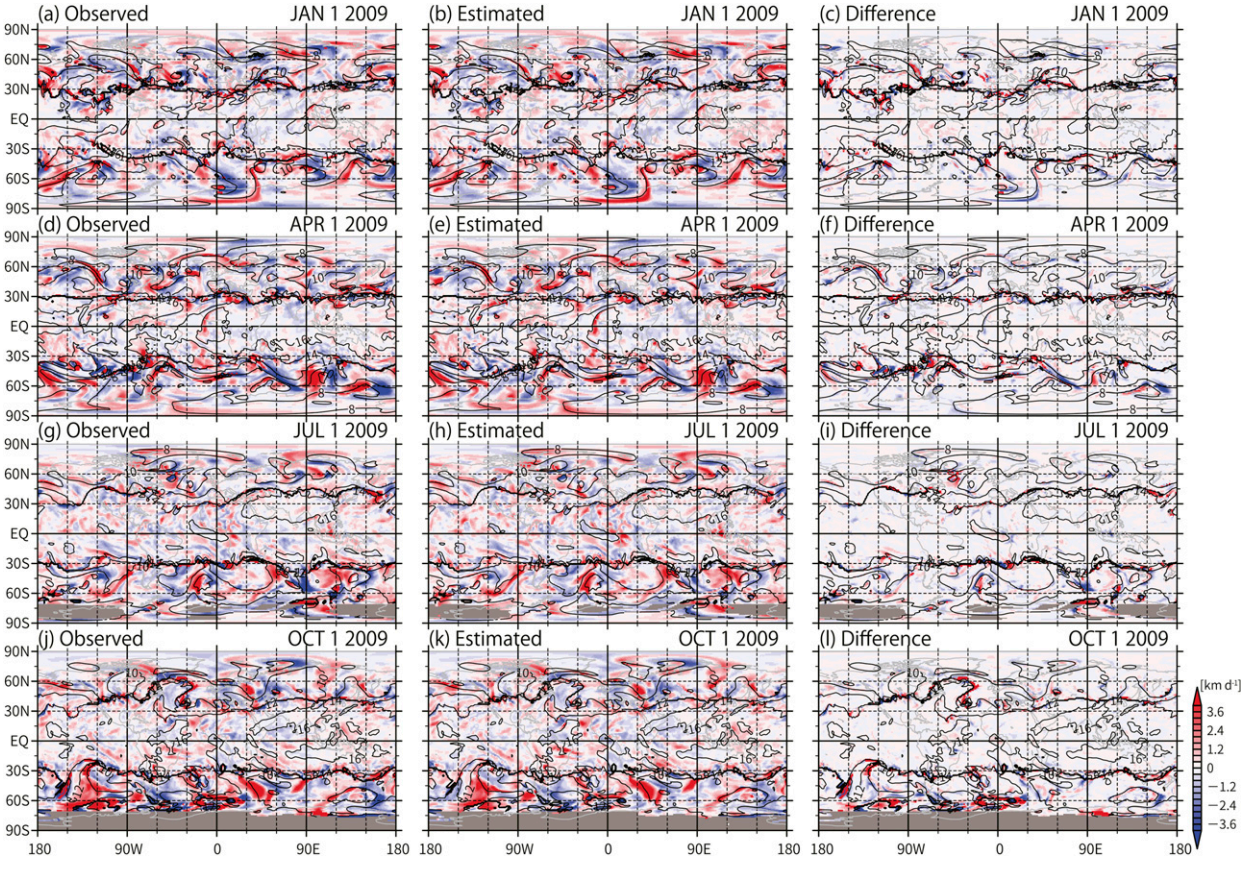

FIG. 11. (a),(d),(g),(j) Horizontal maps of LRT height (contours; interval: 2 km) and its tendency (colors) at 0000 UT (a) 1 Jan, (d) 1 Apr, (g) 1 Jul, and (j) 1 Oct 2009. The gray region indicates where the LRT is undetectable. (b),(e),(h),(k) As in (a), (d), (g), and (j), but for the estimated tendency. (c),(f),(i),(l) As in (a), (d), (g), and (j), but for the difference between the observed and estimated tendencies.

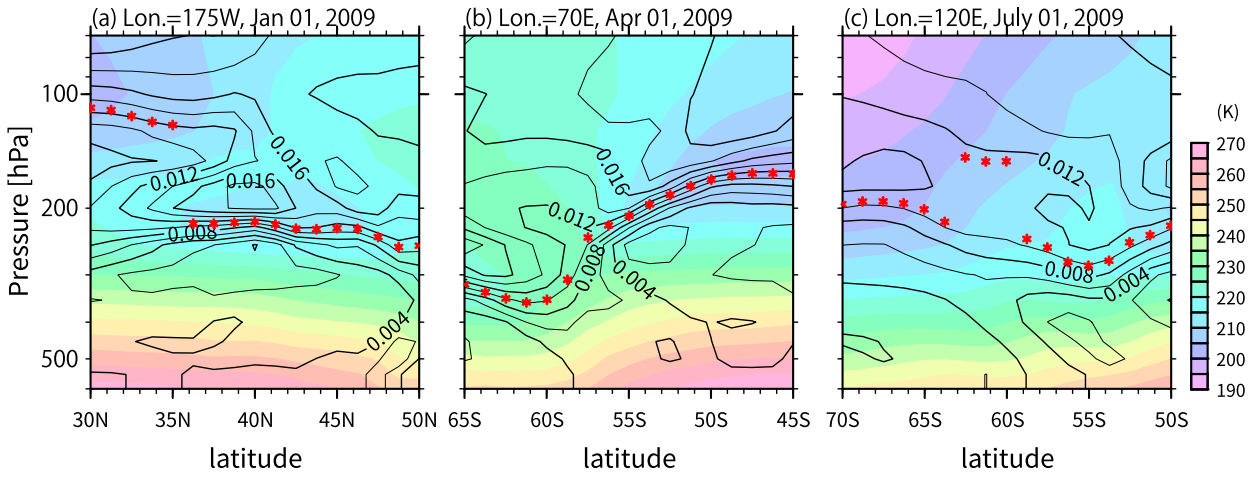

FIG. 12. Latitude–pressure sections of temperature (colors) and $\partial\theta/\partial z$ (contours; interval: 4×10^{-3} K m^{-1}) in (a) 30°–50°N, 175°W on 1 Jan, (b) 65°–45°S, 70°E on 1 Apr, and (c) 70°–50°S, 120°E on 1 Jul. Red stars indicate the LRT.

around 57.5°S, with the height of the LRT considerably decreasing at higher latitudes. This indicates that the tropopause fold likely occurs with the tropospheric front structure. In such a situation, the denominator of Eq. (4) is underestimated, resulting in the large estimates for the tropopause tendency. It is confirmed that the large discrepancies that are likely associated with the tropopause folds are observed in the extratropics in other panels, for example, 45°–60°N, 90°–70°W on 1 January and 45°–60°S, 20°–15°W, on 1 October (not shown). Figure 12c showed the same plot but for in 70°–50°S, 120°E. The locally elevated tropopause is found in 62.5°–60°S. This is likely due to the low temperature in the winter stratosphere. In a similar way, most of the large discrepancies in the southern high latitudes on 1 October are associated with the low temperature in the polar stratosphere (not shown).

The present analyses showed several cases where the observed and estimated tendencies in z_T are significantly different in the reanalysis data: the sharp transition region from the high tropical to the low extratropical LRT, tropopause folds associated with tropospheric fronts, and the polar winter (especially in the Southern Hemisphere). The estimates, nevertheless, considerably accord well with the observed tendency in most of the analyzed region, which indicates that the derived equation can be used sufficiently for quantitative analyses. Note that, since the reanalysis data is gridded at a horizontal resolution of 1.25° × 1.25°, the applicability to phenomena smaller than the resolution is still unknown. Another caveat is that, since reanalysis dataset contains assimilation increments inherently, which is not necessarily small around the tropopause (e.g., Fueglistaler et al. 2009a), the contribution by each term based on Eq. (5) must be carefully quantified.

6. Summary and concluding remarks

The present study derived a diagnostic equation for the LRT heights under the assumption that the tropopause is characterized by a discontinuity in the vertical gradient of the potential temperature. Because the derived equation is kinematic, the zonal-mean version of the relation can be derived unless the transition of θ_z across the tropopause is reasonably smooth.

To examine the validity of the assumptions that are used here, the derived relation was applied to the temporal variations of LRT heights associated with baroclinic waves in an idealized numerical calculation, to the zonal-mean LRT height obtained from GPS radio occultation data, and to temporal variations of LRT heights in reanalysis data. The applications showed that the estimated tendency of the LRT height corresponds well with the observed tendency. Together with the thermodynamic equation, it is possible to quantify the contribution from each term in the equation to the tendency of the LRT heights. In future studies, it would be interesting to examine the time variation of the LRT heights associated with various tropospheric and stratospheric phenomena by applying the diagnostic equations to reanalysis data.

The derived equation includes the sharpness of tropopause, which is considered important for stratosphere–troposphere exchange of air mass. From the derived diagnostic relation [e.g., Eq. (4)], the tendency of the LRT height turns out to be proportional to the inverse of the sharpness. In other words, the heating rate contrasts across the tropopause divided by the sharpness are converted into the tendency of the LRT heights.

Note that other equations including the tendency of the LRT heights can be derived using more complex,

and probably accurate, models of the tropopause. One candidate is the tropopause having a constant depth layer with high static stability above, which mimics the TIL. The resulting relation would include not only the tendency of LRT heights but also that of static stability in the TIL. The tendency equations of the tropopause defined by the potential vorticity or chemical tracers may be useful for analyses for the polar region. It should be emphasized that even though the equation is based on a simplified tropopause having a first-order discontinuity in the potential temperature, the obtained tendency is in a quite good agreement with the observed tendency. This means that the LRT is well approximated by a discontinuity of the vertical gradient in the potential temperature in terms of its temporal change.

Acknowledgments. This study is supported by JSPS KAKENHI Grant JP16K17801/JP19K14791 and JST CREST Grant JPMJCR1663. The COSMIC dry temperature data were provided by the COSMIC Data Analysis and Archive Center (http://cdaac-www.cosmic.ucar.edu/cdaac/). The JRA-55 dataset is available from the JMA Data Dissemination System (http://jra.kishou.go.jp/JRA-55/index_en.html). DCPAM5 are developed by the DCPAM development team and available from https://www.gfd-dennou.org/library/dcpam/index.htm.en. All graphics were drawn by software developed by the Dennou-Ruby Davis project. We thank Ryosuke Shibuya and Arata Amemiya for helpful discussions and comments on this work. The authors acknowledge two anonymous reviewers for greatly helping us to improve this manuscript.

APPENDIX

Another Derivation of Eq. (4)

First, we introduce the following two assumptions: (i) θ_z has a discontinuity at $z = z_T(t)$ $(a < z_T < b)$, but is otherwise a continuous function. (ii) θ is a smooth function except for $z = z_T(t)$. Let us consider the following integral over an interval of (a, b):

$$\int_a^b \frac{\partial\theta}{\partial z}dz = \int_a^{z_T(t)} \frac{\partial\theta}{\partial z}dz + \int_{z_T(t)}^b \frac{\partial\theta}{\partial z}dz. \tag{A1}$$

Taking the Euler derivative of Eq. (A1), the first term of the right-hand side can be rewritten as

$$\frac{\partial}{\partial t}\left[\int_a^{z_T(t)} \frac{\partial\theta}{\partial z}dz\right] = \int_a^{z_T(t)} \frac{\partial}{\partial t}\left(\frac{\partial\theta}{\partial z}\right)dz + \frac{\partial z_T}{\partial t}\frac{\partial\theta}{\partial z}\bigg|_{z_T-0},$$

where $(\partial\theta/\partial z)|_{z_T-0} \equiv \lim_{z\nearrow z_T}(\partial\theta/\partial z)$. Here, Leibniz's integral rule is used:

$$\frac{d}{dt}\left[\int_{p(t)}^{q(t)} f(x,t)\,dx\right] = f[q(t),t]\frac{dq}{dt} - f[p(t),t]\frac{dp}{dt} + \int_{p(t)}^{q(t)} \frac{\partial f}{\partial t}dx$$

Applying Leibniz's rule to the second term on the right-hand side of Eq. (A1), the Euler derivative on the right-hand side of Eq. (A1) is rewritten as follows:

$$\begin{aligned}
&\int_a^{z_T(t)} \frac{\partial}{\partial t}\left(\frac{\partial\theta}{\partial z}\right)dz + \int_{z_T(t)}^b \frac{\partial}{\partial t}\left(\frac{\partial\theta}{\partial z}\right)dz - \frac{\partial z_T}{\partial t}\left[\frac{\partial\theta}{\partial z}\right]_{z_T-0}^{z_T+0} \\
&= \int_a^{z_T(t)} \frac{\partial}{\partial z}\left(\frac{\partial\theta}{\partial t}\right)dz + \int_{z_T(t)}^b \frac{\partial}{\partial z}\left(\frac{\partial\theta}{\partial t}\right)dz - \frac{\partial z_T}{\partial t}\left[\frac{\partial\theta}{\partial z}\right]_{z_T-0}^{z_T+0} \\
&= \left[\frac{\partial\theta}{\partial t}\right]_a^{z_T-0} + \left[\frac{\partial\theta}{\partial t}\right]_{z_T+0}^b - \frac{\partial z_T}{\partial t}\left[\frac{\partial\theta}{\partial z}\right]_{z_T-0}^{z_T+0},
\end{aligned} \tag{A2}$$

where $[f(z)]_a^b \equiv f(b) - f(a)$ and $(\partial\theta/\partial z)|_{z_T+0} \equiv \lim_{z\searrow z_T}(\partial\theta/\partial z)$. Note that the left-hand side of Eq. (A1) is $[\theta]_a^b$ and its Euler derivative is $[\partial\theta/\partial t]_a^b$. Thus, if $[\partial\theta/\partial z]_{z_T-0}^{z_T+0}$ has a finite value, the diagnostic relation is obtained:

$$\frac{\partial z_T}{\partial t} = -\left[\frac{\partial\theta}{\partial t}\right]_{z_T-0}^{z_T+0} \Big/ \left[\frac{\partial\theta}{\partial z}\right]_{z_T-0}^{z_T+0}. \tag{A3}$$

Obviously, Eq. (A3) is equivalent to Eq. (4).

REFERENCES

Andrews, D. G., J. R. Holton, and C. B. Leovy, 1987: *Middle Atmosphere Dynamics*. Academic Press, 489 pp.

Anthes, R. A., and Coauthors, 2008: The COSMIC/*FORMOSAT-3* Mission: Early results. *Bull. Amer. Meteor. Soc.*, **89**, 313–333, https://doi.org/10.1175/BAMS-89-3-313.

Barroso, J. A., and P. Zurita-Gotor, 2016: Intraseasonal variability of the zonal-mean extratropical tropopause: The role of changes in polar vortex strength and upper-troposphere wave breaking. *J. Atmos. Sci.*, **73**, 1383–1399, https://doi.org/10.1175/JAS-D-15-0177.1.

Bethan, S., G. Vaughan, and S. J. Reid, 1996: A comparison of ozone and thermal tropopause heights and the impact of tropopause definition on quantifying the ozone content of the troposphere. *Quart. J. Roy. Meteor. Soc.*, **122**, 929–944, https://doi.org/10.1002/qj.49712253207.

Birner, T., 2006: Fine-scale structure of the extratropical tropopause region. *J. Geophys. Res.*, **111**, D04104, https://doi.org/10.1029/2005JD006301.

——, A. Dörnbrack, and U. Schumann, 2002: How sharp is the tropopause at midlatitudes? *Geophys. Res. Lett.*, **29**, 1700, https://doi.org/10.1029/2002GL015142.

Danielsen, E. F., R. S. Hipskind, W. L. Starr, J. F. Vedder, S. E. Gaines, D. Kley, and K. K. Kelly, 1991: Irreversible transport in the stratosphere by internal waves of short vertical wavelength. *J. Geophys. Res.*, **96**, 17 433–17 452, https://doi.org/10.1029/91JD01362.

Frierson, D. M. W., I. M. Held, and P. Zurita-Gotor, 2006: A gray-radiation aquaplanet moist GCM. Part I: Static stability and eddy scale. *J. Atmos. Sci.*, **63**, 2548–2566, https://doi.org/10.1175/JAS3753.1.

Fueglistaler, S., B. Legras, A. Beljaars, J. J. Morcrette, A. Simmons, A. M. Tompkins, and S. Uppala, 2009a: The diabatic heat budget of the upper troposphere and lower/mid stratosphere in ECMWF reanalyses. *Quart. J. Roy. Meteor. Soc.*, **135**, 21–37, https://doi.org/10.1002/qj.361.

——, A. E. Dessler, T. J. Dunkerton, I. Folkins, Q. Fu, and P. W. Mote, 2009b: Tropical tropopause layer. *Rev. Geophys.*, **47**, RG1004, https://doi.org/10.1029/2008RG000267.

Gettelman, A., and Coauthors, 2010: Multimodel assessment of the upper troposphere and lower stratosphere: Tropics and global trends. *J. Geophys. Res.*, **115**, D00M08, https://doi.org/10.1029/2009jd013638.

——, P. Hoor, L. L. Pan, W. J. Randel, M. I. Hegglin, and T. Birner, 2011: The extratropical upper troposphere and lower stratosphere. *Rev. Geophys.*, **49**, RG3003, https://doi.org/10.1029/2011RG000355.

Grise, K. M., D. W. J. Thompson, and T. Birner, 2010: A global survey of static stability in the stratosphere and upper troposphere. *J. Climate*, **23**, 2275–2292, https://doi.org/10.1175/2009JCLI3369.1.

Hartmann, D. L., J. R. Holton, and Q. Fu, 2001: The heat balance of the tropical tropopause, cirrus, and stratospheric dehydration. *Geophys. Res. Lett.*, **28**, 1969–1972, https://doi.org/10.1029/2000GL012833.

Hegglin, M. I., C. D. Boone, G. L. Manney, and K. A. Walker, 2009: A global view of the extratropical tropopause transition layer from Atmospheric Chemistry Experiment Fourier Transform Spectrometer O_3, H_2O, and CO. *J. Geophys. Res.*, **114**, D00B11, https://doi.org/10.1029/2008jd009984.

——, and Coauthors, 2010: Multimodel assessment of the upper troposphere and lower stratosphere: Extratropics. *J. Geophys. Res.*, **115**, D00M09, https://doi.org/10.1029/2010jd013884.

Held, I. M., 1982: On the height of the tropopause and the static stability of the troposphere. *J. Atmos. Sci.*, **39**, 412–417, https://doi.org/10.1175/1520-0469(1982)039<0412:OTHOTT>2.0.CO;2.

Holton, J. R., and G. J. Hakim, 2012: *An Introduction to Dynamic Meteorology*. 5th ed. International Geophysics Series, Vol. 88, Academic Press, 552 pp.

Hoskins, B. J., M. E. McIntyre, and A. W. Robertson, 1985: On the use and significance of isentropic potential vorticity maps. *Quart. J. Roy. Meteor. Soc.*, **111**, 877–946, https://doi.org/10.1002/qj.49711147002.

Johnson, R. H., 1986: Short-term variations of the tropopause height over the winter MONEX area. *J. Atmos. Sci.*, **43**, 1152–1163, https://doi.org/10.1175/1520-0469(1986)043<1152:STVOTT>2.0.CO;2.

Juckes, M., 1994: Quasi-geostrophic dynamics of the tropopause. *J. Atmos. Sci.*, **51**, 2756–2768, https://doi.org/10.1175/1520-0469(1994)051<2756:QDOTT>2.0.CO;2.

——, 1997: The mass flux across the tropopause: Quasi-geostrophic theory. *Quart. J. Roy. Meteor. Soc.*, **123**, 71–99, https://doi.org/10.1002/qj.49712353703.

Keyser, D., and M. A. Shapiro, 1986: A review of the structure and dynamics of upper-level frontal zones. *Mon. Wea. Rev.*, **114**, 452–499, https://doi.org/10.1175/1520-0493(1986)114<0452:AROTSA>2.0.CO;2.

Kobayashi, S., and Coauthors, 2015: The JRA-55 reanalysis: General specifications and basic characteristics. *J. Meteor. Soc. Japan*, **93**, 5–48, https://doi.org/10.2151/jmsj.2015-001.

Kohma, M., and K. Sato, 2014: Variability of upper tropospheric clouds in the polar region during stratospheric sudden warmings. *J. Geophys. Res. Atmos.*, **119**, 10 100–10 113, https://doi.org/10.1002/2014JD021746.

Li, Y., and D. W. J. Thompson, 2013: The signature of the stratospheric Brewer-Dobson circulation in tropospheric clouds. *J. Geophys. Res. Atmos.*, **118**, 3486–3494, https://doi.org/10.1002/jgrd.50339.

Lilly, D. K., 1968: Models of cloud-topped mixed layers under a strong inversion. *Quart. J. Roy. Meteor. Soc.*, **94**, 292–309, https://doi.org/10.1002/qj.49709440106.

Norton, W. A., 2006: Tropical wave driving of the annual cycle in tropical tropopause temperatures. Part II: Model results. *J. Atmos. Sci.*, **63**, 1420–1431, https://doi.org/10.1175/JAS3698.1.

Pan, L. L., and L. A. Munchak, 2011: Relationship of cloud top to the tropopause and jet structure from CALIPSO data. *J. Geophys. Res.*, **116**, D12201, https://doi.org/10.1029/2010JD015462.

——, S. B. Honomichl, T. V. Bui, T. Thornberry, A. Rollins, E. Hintsa, and E. J. Jensen, 2018: Lapse rate or cold point: The tropical tropopause identified by in situ trace gas measurements. *Geophys. Res. Lett.*, **45**, 10 756–10 763, https://doi.org/10.1029/2018GL079573.

Polvani, L. M., R. K. Scott, and S. J. Thomas, 2004: Numerically converged solutions of the global primitive equations for testing the dynamical core of atmospheric GCMs. *Mon. Wea. Rev.*, **132**, 2539–2552, https://doi.org/10.1175/MWR2788.1.

Randel, W. J., and E. J. Jensen, 2013: Physical processes in the tropical tropopause layer and their roles in a changing climate. *Nat. Geosci.*, **6**, 169–176, https://doi.org/10.1038/ngeo1733.

——, F. Wu, and D. J. Gaffen, 2000: Interannual variability of the tropical tropopause derived from radiosonde data and NCEP reanalyses. *J. Geophys. Res.*, **105**, 15 509–15 523, https://doi.org/10.1029/2000JD900155.

——, ——, and P. Forster, 2007a: The extratropical tropopause inversion layer: Global observations with GPS data, and a radiative forcing mechanism. *J. Atmos. Sci.*, **64**, 4489–4496, https://doi.org/10.1175/2007JAS2412.1.

——, D. J. Seidel, and L. L. Pan, 2007b: Observational characteristics of double tropopauses. *J. Geophys. Res.*, **112**, D07309, https://doi.org/10.1029/2006JD007904.

——, R. Garcia, and F. Wu, 2008: Dynamical balances and tropical stratospheric upwelling. *J. Atmos. Sci.*, **65**, 3584–3595, https://doi.org/10.1175/2008JAS2756.1.

Reichler, T., M. Dameris, and R. Sausen, 2003: Determining the tropopause height from gridded data. *Geophys. Res. Lett.*, **30**, 2042, https://doi.org/10.1029/2003GL018240.

Schmidt, T., S. Heise, J. Wickert, G. Beyerle, and C. Reigber, 2005: GPS radio occultation with CHAMP and SAC-C: Global monitoring of thermal tropopause parameters. *Atmos. Chem. Phys.*, **5**, 1473–1488, https://doi.org/10.5194/acp-5-1473-2005.

Schneider, T., 2004: The tropopause and the thermal stratification in the extratropics of a dry atmosphere. *J. Atmos. Sci.*, **61**, 1317–1340, https://doi.org/10.1175/1520-0469(2004)061<1317:TTATTS>2.0.CO;2.

Schreiner, W., C. Rocken, S. Sokolovskiy, S. Syndergaard, and D. Hunt, 2007: Estimates of the precision of GPS radio occultations from the COSMIC/*FORMOSAT-3* mission. *Geophys. Res. Lett.*, **34**, L04808, https://doi.org/10.1029/2006GL027557.

Seidel, D. J., R. J. Ross, J. K. Angell, and G. C. Reid, 2001: Climatological characteristics of the tropical tropopause as revealed by radiosondes. *J. Geophys. Res.*, **106**, 7857–7878, https://doi.org/10.1029/2000JD900837.

Shepherd, M. G., and T. Tsuda, 2008: Large-scale planetary disturbances in stratospheric temperature at high-latitudes in the southern summer hemisphere. *Atmos. Chem. Phys.*, **8**, 7557–7570, https://doi.org/10.5194/acp-8-7557-2008.

Shibuya, R., K. Sato, Y. Tomikawa, M. Tsutsumi, and T. Sato, 2015: A study of multiple tropopause structures caused by inertia–gravity waves in the Antarctic. *J. Atmos. Sci.*, **72**, 2109–2130, https://doi.org/10.1175/JAS-D-14-0228.1.

Son, S. W., S. Lee, and S. B. Feldstein, 2007: Intraseasonal variability of the zonal-mean extratropical tropopause height. *J. Atmos. Sci.*, **64**, 608–620, https://doi.org/10.1175/JAS3855.1.

——, N. F. Tandon, and L. M. Polvani, 2011: The fine-scale structure of the global tropopause derived from COSMIC GPS radio occultation measurements. *J. Geophys. Res.*, **116**, D20113, https://doi.org/10.1029/2011JD016030.

Steinbrecht, W., H. Claude, U. Kohler, and K. P. Hoinka, 1998: Correlations between tropopause height and total ozone: Implications for long-term changes. *J. Geophys. Res.*, **103**, 19 183–19 192, https://doi.org/10.1029/98JD01929.

Takahashi, Y. O., and Coauthors, 2018: DCPAM: Planetary atmosphere model. Dennou-Club Planetary Atmospheric Model Project, http://www.gfd-dennou.org/library/dcpam/.

Tanaka, M., 2017: *Physics of Nonlinear Waves* (in Japanese). Morikita Publishing, 245 pp.

Thompson, D. W. J., S. Bony, and Y. Li, 2017: Thermodynamic constraint on the depth of the global tropospheric circulation. *Proc. Natl. Acad. Sci. USA*, **114**, 8181–8186, https://doi.org/10.1073/pnas.1620493114.

Thorncroft, C. D., B. J. Hoskins, and M. F. Mcintyre, 1993: Two paradigms of baroclinic-wave life-cycle behavior. *Quart. J. Roy. Meteor. Soc.*, **119**, 17–55, https://doi.org/10.1002/qj.49711950903.

Thuburn, J., and G. C. Craig, 1997: GCM tests of theories for the height of the tropopause. *J. Atmos. Sci.*, **54**, 869–882, https://doi.org/10.1175/1520-0469(1997)054<0869:GTOTFT>2.0.CO;2.

——, and ——, 2000: Stratospheric influence on tropopause height: The radiative constraint. *J. Atmos. Sci.*, **57**, 17–28, https://doi.org/10.1175/1520-0469(2000)057<0017:SIOTHT>2.0.CO;2.

Tomikawa, Y., K. Sato, and T. G. Shepherd, 2006: A diagnostic study of waves on the tropopause. *J. Atmos. Sci.*, **63**, 3315–3332, https://doi.org/10.1175/JAS3800.1.

——, Y. Nishimura, and T. Yamanouchi, 2009: Characteristics of tropopause and tropopause inversion layer in the polar region. *SOLA*, **5**, 141–144, https://doi.org/10.2151/sola.2009-036.

Wirth, V., 2000: Thermal versus dynamical tropopause in upper-tropospheric balanced flow anomalies. *Quart. J. Roy. Meteor. Soc.*, **126**, 299–317, https://doi.org/10.1002/qj.49712656215.

WMO, 1957: Definition of the tropopause. *WMO Bull.*, **6**, 136–140.

Yulaeva, E., J. R. Holton, and J. M. Wallace, 1994: On the cause of the annual cycle in tropical lower-stratospheric temperatures. *J. Atmos. Sci.*, **51**, 169–174, https://doi.org/10.1175/1520-0469(1994)051<0169:OTCOTA>2.0.CO;2.

Zängl, G., and K. P. Hoinka, 2001: The tropopause in the polar regions. *J. Climate*, **14**, 3117–3139, https://doi.org/10.1175/1520-0442(2001)014<3117:TTITPR>2.0.CO;2.

Zeman, O., and H. Tennekes, 1977: Parameterization of turbulent energy budget at top of daytime atmospheric boundary-layer. *J. Atmos. Sci.*, **34**, 111–123, https://doi.org/10.1175/1520-0469(1977)034<0111:POTTEB>2.0.CO;2.

Zurita-Gotor, P., and G. K. Vallis, 2013: Determination of extratropical tropopause height in an idealized gray radiation model. *J. Atmos. Sci.*, **70**, 2272–2292, https://doi.org/10.1175/JAS-D-12-0209.1.